IEEE Access
Multidisciplinary | Rapid Review | Open Access Journal

Received May 15, 2018, accepted June 16, 2018, date of publication June 19, 2018, date of current version July 6, 2018.

Digital Object Identifier 10.1109/ACCESS.2018.2849010

Random Positional Deviations Correction for Each LED via ePIE in Fourier Ptychographic Microscopy

SINING CHEN[1], TINGFA XU[1,2], JIZHOU ZHANG[1], XING WANG[1], AND YIZHOU ZHANG[1]

[1]Image Engineering & Video Technology Lab, School of Optics and Photonics, Beijing Institute of Technology, Beijing 100081, China
[2]Key Laboratory of Photoelectronic Imaging Technology and System, Ministry of Education of China, Beijing 100081, China

Corresponding author: Tingfa Xu (ciom_xtf1@bit.edu.cn)

This work was supported in part by the Major Science Instrument Program of the National Natural Science Foundation of China under Grant 61527802 and in part by the General Program of National Natural Science Foundation of China under Grant 61371132 and Grant 61471043.

ABSTRACT Fourier ptychography microscopy (FPM) is a lately developed technique, which achieves wide field, high resolution, and phase imaging, simultaneously. FPM stitches together the captured low-resolution images corresponding to angular varying illuminations in Fourier domain utilizing the concept of synthetic aperture and phase retrieval algorithms, which can surpass the space-bandwidth product limit of the objective lens and reconstruct a high-resolution complex image. In general FPM system, the LED source is important for the reconstructed quality and it is sensitive to the positions of each LED element. We find that the random positional deviations of each LED element can bring errors in reconstructed results, which is relative to a feedback parameter. To improve the reconstruction rate and correct random deviations, we combine an initial phase guess and a feedback parameter based on differential phase contrast and extended ptychographical iterative engine to propose an optimized iteration process for FPM. The simulated and experimental results indicate that the proposed method shows the reliability and validity towards the random deviations yet accelerates the convergence. More importantly, it is verified that this method can accelerate the convergence, reduce the requirement of LED array accuracy, and improve the quality of the reconstructed results.

INDEX TERMS Computational imaging, imaging system, microscopy, phase retrieval.

I. INTRODUCTION

Fourier ptychographic (FP) [1]–[3] is a computational imaging technique, which aims to recover sample's high-resolution (HR) complex (amplitude and phase) information and acquire wide field-of-view (FOV), although only intensity data are measured. It is based on the concept of ptychography [4]–[6] which overcomes the physical space-bandwidth-product (SBP) limit. Instead of moving a limited-size illumination probe sequentially in conventional ptychography, it uses a LED array source to obtain different illumination oblique plane waves. Then a set of low-resolution (LR) intensity images of the specimen with quantitative overlap are recorded and their corresponding components can be iteratively combined in Fourier domain to realize synthetic aperture [7]–[9] and phase retrieval [10]–[14]. Recently, the application of FP in microscopic imaging, termed Fourier ptychographic microscopy (FPM) has been introduced [15]. As a result, the diffraction limit of the objective can be expanded and the SBP of microscope can be boosted. Besides, because of the non-interferometric phase retrieval technique, a HR complex image can be reconstructed. The resolution of the final reconstructed image is determined by the sum of synthetic-aperture (objective lens and illumination NAs) [6]. Because FPM is a kind of label-free imaging offering the HR and wide FOV complex images, numerous applications [17]–[20] have been implemented in it within a few years.

In conventional FPM, alternating projections (AP) which updates the objective function between the space and Fourier domain iteratively is widely used. However, it is sensitive to noises and positional errors. In order to optimize the original FPM, some studies have been reported [21]–[31]. On the one hand, because of the long acquisition time for measured images, it limits the application in real-time observation. Thereby, some studies aim to reduce the acquisition time effectively [21]–[23]. The multiplexed coded illumination, sparsely sampled strategies and content adaptive illumination method have been demonstrated to reduce the acquisition time effectively. On the other hand, more and more noise-robust and system aberrations correction algorithms have

been proposed to improve the accuracy of reconstructed results. Some studies have adopted other phase retrieval algorithms to replace the AP process, such as Wirtinger flow optimization (WFP) [24] which is suitable for Gaussian noise. Some have also proposed fast gradational reconstruction to adapt noises and improve convergence [25], embedded pupil function recovery to update pupil function [26] and threshold model to correct noises and aberrations [27]. Furthermore, similar to the probe of conventional ptychography, the sample and illuminating LED matrix are both positional fixed while each LED is used for illuminating during the images acquisition process in FPM platform. Thus the positioning errors of LEDs, which will bring distorted information into captured raw images, is an essential systematic aberration in FP settings. The conjugate gradient [13] and the annealing [28] ptychographic correction algorithm have been developed. Recently, the efficient positional misalignment correction method (pcFPM) has been proposed based on the simulated annealing (SA) algorithm [29]. It introduces a global positional misalignment model of the LED matrix and updates LED position estimate. And it is valid for global LED matrix misplaced. However, there are some random deviations during the manufacturing and welding process of each LED. It can generate unequal interval LED elements and introduce distortion to the reconstructed results. So the conventional recovery quality and the convergence will be degraded. Consequently, it is essential to correct random positional deviations of each LED and keep a fast convergence in current FPM platforms.

In order to correct the random positional deviations, we propose a correction approach for each LED element with random positional deviations, termed rpcFPM, based on the ePIE [14] and DPC [30], [31] algorithm which is a quantitative phase retrieval technique employed in optical imaging. After each iteration, rpcFPM calculates the cross correlation coefficient of objective function between two adjacent iterations and adjust the feedback parameter according to the coefficient value. The position shift and the corrected position of each LED are also expressed in the iterative process. Furthermore, an objective function relaxation constraint is introduced for the new reconstruction framework to suppress noise slightly. In addition, to improve the recovering efficiency of the proposed method, recovered DPC phase information is utilized as an initial phase guess. After initializing the DPC phase as the phase guess, all the captured images are iterated under different feedback parameter in the next iteration with objective function constraint. In this work, we evaluate rpcFPM and conventional FPM reconstructed results in simulations and experiments. All the results and corrected reconstructed images demonstrate that using our rpcFPM can achieve proper correction.

The whole article is structured as follows: First, we introduce the FPM platform and the images acquisition module, describe the conventional FPM algorithm, and then propose the iterative process rpcFPM with feedback parameter and DPC initial phase guess to correct random positional deviations of each LED element based on the ePIE algorithm. In the next two sections, simulation, experimental results and the conclusion are presented respectively.

II. THEORIES AND METHODS

A. SYSTEM AND IMAGES ACQUISITION

Firstly, let us review the FPM system and the images acquisition. Fig.1 (a) shows the FPM system which consists of LED matrix illumination, sample, low-power objective lens, tube lens and a CMOS camera. The LED matrix is controlled by an Arduino circuit board shown in Fig. 1 (c) and each LED illuminates the sample with an oblique plane wave vector (as shown in Fig.1 (b)). In this work, the images acquisition process contains two parts: images for DPC retrieval and images for FPM reconstruction. In order to set the center of LED matrix to the middle of the objective lens, we use a simple method in brightfield localization (BFL) [32] to adjust the LED matrix. In this adjustment process, we just use the 3×3 middle LEDs which are in brightfield and the corresponding captured images are shown in Fig.2 (a). The boundary of the system setup and LED matrix are expressed as red circle and orange dotted line respectively. We can see that the center of the LED matrix is misaligned from the center of system and the blue board line between brightfield and darkfield is asymmetric. So we adjust the position of the central LEDs to the middle roughly and the captured images are shown in Fig. 2 (b) whose borders are symmetrical. Then, we control the Arduino circuit board to obtain four types of

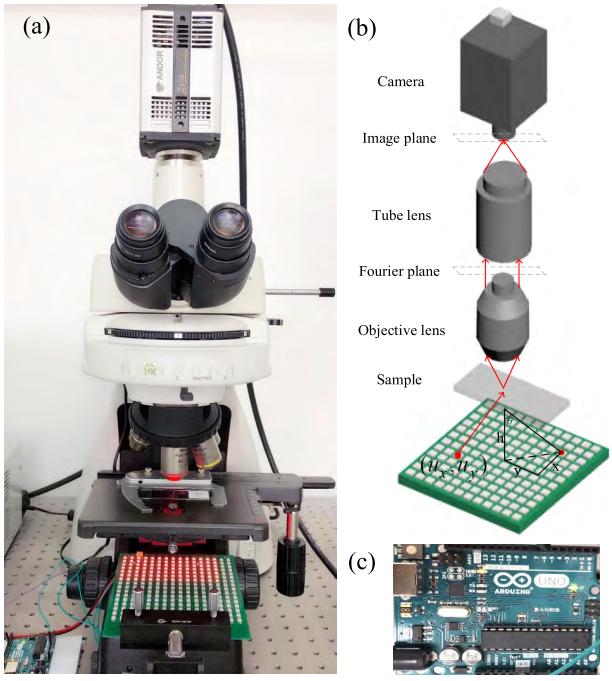

FIGURE 1. Experimental platform. (a) The actual experimental platform on a Nikon eclipse microscope. (b) The module of FPM system and the imaging process. (c) The controller of the LED array.

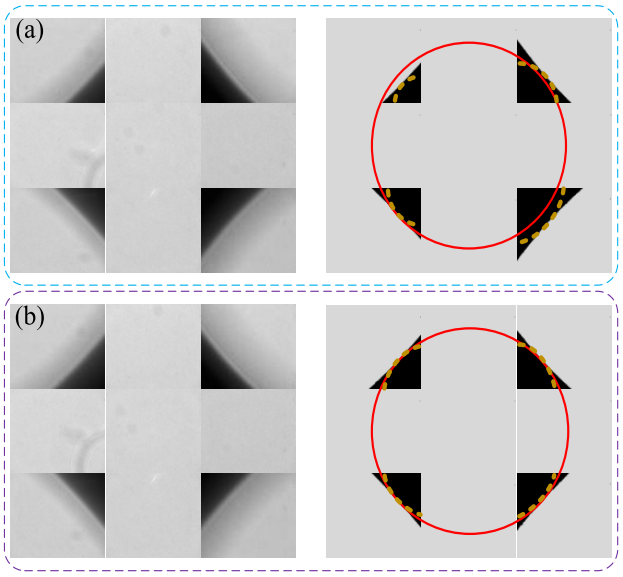

FIGURE 2. The images captured by LEDs in brightfield. (a) shows the captured images with misalignment and the boundary of brightfield and darkfield. (b) shows the images after calibrating LED array and the corresponding boundary.

illumination and capture the corresponding images as shown in Fig. 3 (b). Finally, Fig. 3 (a) shows that we light each LED in turn and 169 images are captured.

B. CONVENTIONAL FPM ALGORITHM

To illustrate the initial phase guess and the random positional deviations of each LED element, we first describe the conventional FPM process. Fig. 1 (b) is the simplified imaging process as described in [15]. It is shown that each LED element is an oblique plane wave vector described as $\mathbf{u}_j = (u_x, u_y)$ $(j = 1, 2, \cdots, N_{img})$. Then this plane wave reaches the specimen which is seen as a thin sample. So $O(\mathbf{r})$ can be expressed as the objective function in real-special plane and $O(\mathbf{u})$ is in image plane. Except the on-axis-illuminate LED, the wave of other LEDs, whose position is $\mathbf{s}_j$, passing through the sample is a shifted version $O(\mathbf{u} - \mathbf{u}_j, \mathbf{s}_j)$ in the exit field. Next, the objective is equivalent to a low pass filter and its corresponding objective pupil function is $P(\mathbf{u})$. So in the Fourier image plane, the complex image can be described as $\psi_j(\mathbf{u}, \mathbf{s}_j) = P(\mathbf{u})O(\mathbf{u} - \mathbf{u}_j, \mathbf{s}_j)$. And each frequency spectrum information passes through the tube lens and inverses Fourier transform to reach the image plane and the camera. In the real-space, the corresponding estimated LR intensity image is expressed as

$$E_j(\mathbf{r}, \mathbf{s}_j) = |\mathcal{F}^{-1}\left\{\psi_j(\mathbf{u}, \mathbf{s}_j)\right\}|^2. \tag{1}$$

where $\mathcal{F}^{-1}$ is the inverse Fourier transform. According to the concept of FPM, the HR complex field can be recovered from a set of LR captured intensity images $I_j(\mathbf{r}, \mathbf{s}_j)$ following an iterative algorithm which updates the space spectrum by replacing the estimated amplitudes with the $I_j(\mathbf{r}, \mathbf{s}_j)$ and keeping the phase information unchanged. And the process is called intensity constraint and expressed as

$$\psi_j^u(\mathbf{r} - \mathbf{r}_j, \mathbf{s}_j) = \sqrt{I_j(\mathbf{r}, \mathbf{s}_j)}\frac{\mathcal{F}^{-1}\left\{\psi_j(\mathbf{u}, \mathbf{s}_j)\right\}}{\sqrt{E_j(\mathbf{r}, \mathbf{s}_j)}}. \tag{2}$$

here we use $\psi_j^u(\mathbf{r} - \mathbf{r}_j, \mathbf{s}_j)$ as the updated complex amplitude sub-image. Then this sub-image is transferred to the corresponding frequency region and the updated sub-spectrum can be described as

$$\psi_j^u(\mathbf{u} - \mathbf{u}_j, \mathbf{s}_j) = P(\mathbf{u}, \mathbf{s}_j)\mathcal{F}\left\{\psi^u(\mathbf{r} - \mathbf{r}_j, \mathbf{s}_j)\right\}. \tag{3}$$

where $\mathcal{F}$ is the Fourier transform. As Fig. 3 (a) shows, by selecting other sub-regions N_{img} times, the HR intensity

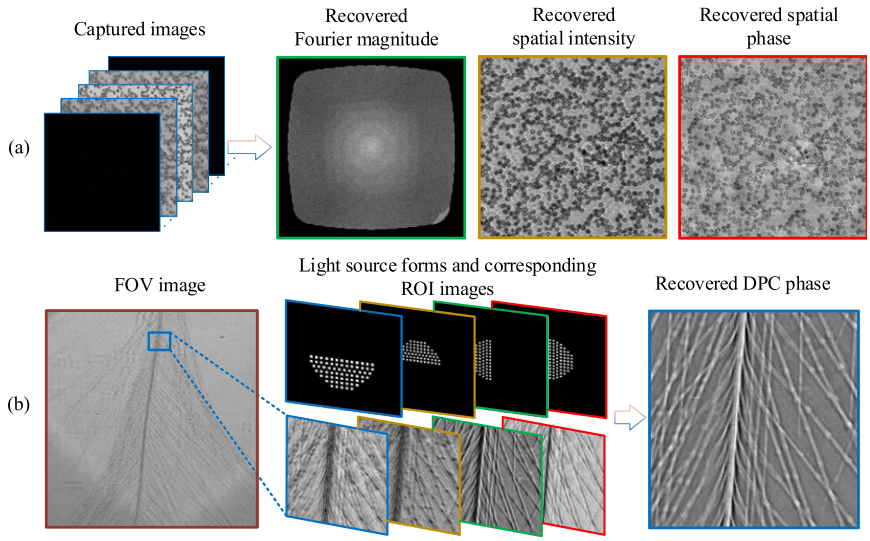

FIGURE 3. The example of conventional FPM and DPC method. (a) The raw captured images and reconstruction results of FPM. (b) The raw image, light source forms and corresponding ROI images and the reconstruction results of DPC.

and phase images can be extracted from the whole updated spectrum.

Generally, in the above-mentioned conventional FPM reconstruction, the initial intensity guess is LR on-axis-illuminated image and the phase is zero. Thus, the reconstructed quality and convergence are affected by the choice of the initial value directly. Besides, because of the low objective NA, the illumination angles of bright-field LED elements are small and low-frequency phase information is poorly captured. Same as the high-frequency information of intensity images, it is difficult to reconstruct low-frequency phase information. So a better recovered phase as the initial phase can not only improve convergence, but also reconstruct the low-frequency phase components correctly. Moreover, in FPM platform, different LED elements have different oblique plane waves $\mathbf{u}_j$ and correspond to different objective functions $O(\mathbf{u}-\mathbf{u}_j, \mathbf{s}_j)$ while each LED element is determined by the specified distance and position. The accurate knowledge of each LED's position is essential for high reconstructed quality. In FPM, even though the distance between adjacent LEDs is set to the same value, there are also some errors and deviations during the manufacturing operation and experimental process. Although we have adjusted the center LED to the middle and the whole LED matrix has been centrosymmetric, each LED element has different deviations for the specified position. We call these deviations as random positional deviations of each LED element which can bring about significant distortion in FPM reconstruction. Hence the random positional deviations correction for each LED element is important in FPM platform.

C. ITERATIVE PROCESS OF RPCFPM

Based on the developed reconstruction scheme for ptychography in [14] and [31], we propose a correction method, termed rpcFPM, to improve the convergence and correct the random positional deviations of each LED element. In rpcFPM, the feedback parameter and the recovered DPC phase $\omega(\mathbf{u})$ are applied in the iterative process. The objective function constraint is further introduced for the new framework. Fig. 4 is a flow chart of rpcFPM and the specific process is shown as follows.

Firstly, we define the pupil function of the setup which is a low-pass filter. And after images acquisition, the light source function is produced and the four intensity images (Top $I_T(\mathbf{r})$, Bellow $I_B(\mathbf{r})$, Left $I_L(\mathbf{r})$, Right $I_R(\mathbf{r})$) are obtained as shown in Fig. 3 (b). And the four images are calculated to get differential intensity images as

$$\begin{cases} I_{D,1}(\mathbf{r}) = \dfrac{I_T(\mathbf{r}) - I_B(\mathbf{r})}{I_T(\mathbf{r}) + I_B(\mathbf{r})} \\ I_{D,2}(\mathbf{r}) = \dfrac{I_L(\mathbf{r}) - I_R(\mathbf{r})}{I_L(\mathbf{r}) + I_R(\mathbf{r})} \end{cases} \tag{4}$$

Then, through the distribution of light source $S(\mathbf{u})$ and pupil function $P(\mathbf{u})$, the phase transfer function $H(\mathbf{u})$ can be calculated as described in [30]. Because each LED element is treated as a coherent point source, the estimated

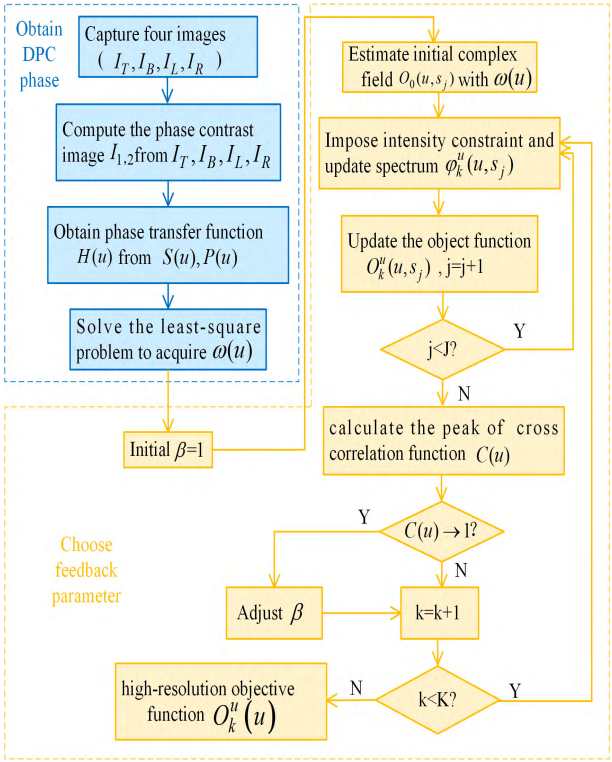

FIGURE 4. The flow diagram of the rpcFPM method.

DPC phase $\omega(\mathbf{u})$ can be transfered as

$$I_D(\mathbf{u}) = \{H(\mathbf{u}) \bullet \omega(\mathbf{u})\}. \tag{5}$$

where $I_D(\mathbf{u})$ is the estimated intensity image. By minimizing the difference between the estimated $I_D(\mathbf{u})$ and calculated $I_{D,i}(\mathbf{u})(i = 1, 2)$ intensities as follows,

$$min\, f(\mathbf{u}) = \left\| I_{D,i}(\mathbf{u}) - I_D(\mathbf{u}) \right\|_2. \tag{6}$$

the DPC deconvolution phase $\omega(\mathbf{u})$ can be acquired. The recovered phase result is shown in Fig. 3 (b). The raw sample is feather, the region of interest under four light source forms are fuzzy but the recovered DPC phase is high-resolution.

Next, the initial guess of intensity and phase are provided and the corresponding initial objective function is set to

$$O_0(\mathbf{u}) = \mathcal{F}\{\sqrt{I_{Cen}(\mathbf{r})} \bullet \exp(j\omega(\mathbf{r}))\}. \tag{7}$$

where $I_{Cen}(\mathbf{r})$ represents the intensity of on-axis-illuminated and $\omega(\mathbf{r})$ is phase image in spatial domain. Using the objective function $O_0(\mathbf{u})$ and imposing intensity constraint as Eq. (2), the spectrum $\psi_{j,k}^u(\mathbf{u}, \mathbf{s}_j)$ can be updated. In order to reconstruct $O(\mathbf{u}, \mathbf{s}_j)$ based on ePIE, we should minimize the cost function as follows.

$$\delta = min\, f(O) = ((P(\mathbf{u})O_k^u(\mathbf{u}, \mathbf{s}_j) - \psi_k(\mathbf{u}, \mathbf{s}_j))). \tag{8}$$

To adjust the reconstructed objective function slightly, we further introduce the objective function relaxation constraint into Eq. (8) and the model can be optimized as

$$f(O) = (\|PO_k - \psi_k\|_2 + \lambda\|O_k\|_2). \tag{9}$$

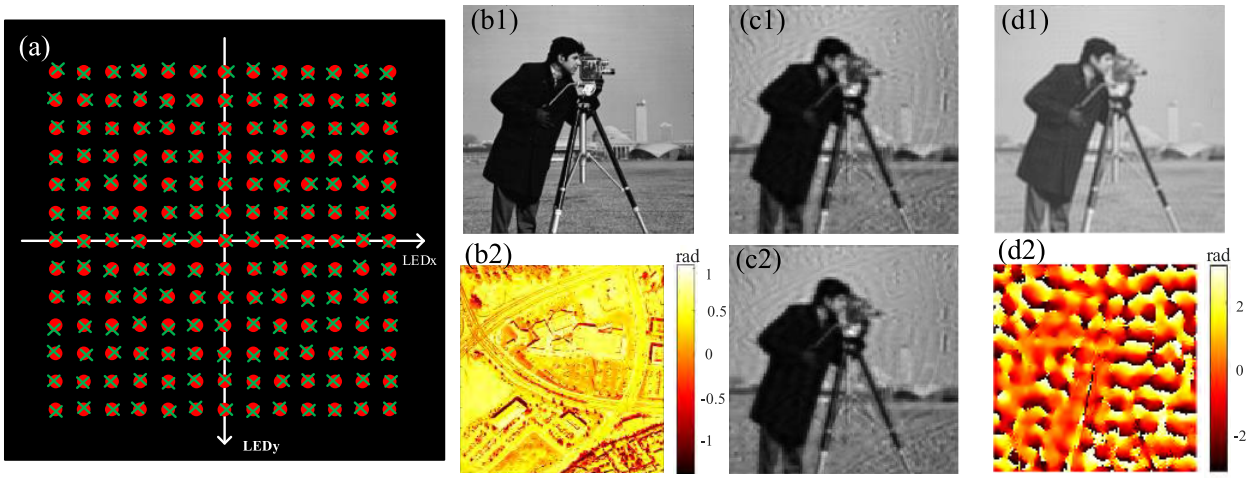

FIGURE 5. An example of complex images with standard location and positional deviations. (a) The random LEDs positional deviations. (b1)-(b2) The true high-resolution intensity and phase images. (c1)-(c2) The simulated images without and with random deviations. (d1)-(d2) The on-axis-illuminated intensity and phase images with LEDs positional deviations for FPM reconstruction.

where λ is a regularization coefficient to prevent the model from overfitting. In implementation, the objective function is updated as

$$O^u_{k+1}\left(\mathbf{u}, \mathbf{s}_j\right) = O^u_k\left(\mathbf{u}, \mathbf{s}_j\right) + \gamma \frac{\partial f(O)}{\partial O^*}. \tag{10}$$

Here the feedback parameter γ is the gradient descent step. And the first derivative of $f(O)$ can be expressed as

$$\frac{\partial f(O)}{\partial O^*} = (P^*(\mathbf{u})(P(\mathbf{u})O^u_k\left(\mathbf{u}, \mathbf{s}_j\right) - \psi_k(\mathbf{u}, \mathbf{s}_j)) + \lambda O^u_k\left(\mathbf{u}, \mathbf{s}_j\right)). \tag{11}$$

where $P^*(\mathbf{u})$ represents the conjugate of $P(\mathbf{u})$. Therefore, the corresponding objective function $O^u\left(\mathbf{u}, \mathbf{s}_j\right)$ according to Eq. (10) can be updated as

$$O^u_{k+1}\left(\mathbf{u}, \mathbf{s}_j\right) = O^u_k\left(\mathbf{u}, \mathbf{s}_j\right) + \gamma(P^*(\mathbf{u})(P(\mathbf{u})O^u_k\left(\mathbf{u}, \mathbf{s}_j\right) - \psi_k(\mathbf{u}, \mathbf{s}_j)) + \lambda O^u_k\left(\mathbf{u}, \mathbf{s}_j\right)). \tag{12}$$

where

$$\gamma = \frac{\beta(\mathbf{s}_k, \mathbf{s})}{|P(\mathbf{u})|^2_{\max}}. \tag{13}$$

In this model, $\beta(\mathbf{s}_k, \mathbf{s})$ denotes an adaptive feedback parameter of positional deviations and $|P(\mathbf{u})|^2_{\max}$ represents a normalization matrix. Normally, to complete one iteration, all the 169 images corresponding to each LED should be updated. The feedback parameter plays an important role in positional correction, which is often set as a constant value in ePIE. However, in this scheme, it is an alterable parameter which is relative to the positions. Actually, the feedback parameter represents the amount and region of information used in the next iteration from the previous estimate. In Eq. (12), when the incremental quantity dwindles gradually, the objective function of the adjacent iterations becomes more similar. Because the object estimate $O(\mathbf{u}, \mathbf{s}_j)$ is related to the position of each LED element, the random positional deviations can bring some distortion into the updated objective function during each iteration. In such condition, the feedback information of each LED is different and the correlation between adjacent iterations is poor.

Finally, in order to acquire the corrected position of each LED in the iterative process, we add the following after the updated objective function.

$$\mathbf{s}_{j,k+1} = \mathbf{s}_{j,k} + \beta\mathbf{\Delta}. \tag{14}$$

where $\mathbf{\Delta}$ is expressed as positional shift of the corresponding LED element between $O^u_{k+1}(\mathbf{u}, \mathbf{s}_j)$ and $O^u_k(\mathbf{u}, \mathbf{s}_j)$, which acquired from the peak value of the cross correlation function. And, the correlation coefficient value also can reflect whether the positional deviations are corrected. Thus, the correlation coefficient value of $O^u_{k+1}(\mathbf{u}, \mathbf{s}_j)$ and $O^u_k(\mathbf{u}, \mathbf{s}_j)$ is calculated to adjust the feedback parameter.

$$\begin{aligned} C(\mathbf{u}) &= O^u_{k+1}(\mathbf{0}, \mathbf{0}) \otimes O^u_k(\mathbf{0}, \mathbf{0}) \\ &= \iint O^u_{k+1}(\mathbf{u}_x, \mathbf{u}_y)O^u_k(\mathbf{u}_x, \mathbf{u}_y)d\mathbf{u}_x d\mathbf{u}_y. \end{aligned} \tag{15}$$

where $\otimes$ represents the convolution and $(\mathbf{u}_x, \mathbf{u}_y)$ is the frequency domain coordinate of the pixel index. It can be seen that the objective function relevance is greater, the positional deviations level $\mathbf{\Delta}$ are lower and the errors between the corrected position $\mathbf{s}_{j,k+1}$ and the ideal position $\mathbf{s}$ are smaller. In other words, when $C(\mathbf{u})$ becomes greater than a threshold, it means the random deviations are nearly corrected and the objective function is more and more accurate. Thus, during the next iteration process, the used information can be decreased for convergence and the corresponding region is more similar to each other. In this case, the feedback parameter is set to $\frac{\beta}{2}$ in the next iteration. On the contrary, feedback parameter is invariant.

$$\beta = \begin{cases} \beta/2, & C(\mathbf{u}) \geq \textit{threshold} \\ \beta, & \textit{otherwise} \end{cases} \tag{16}$$

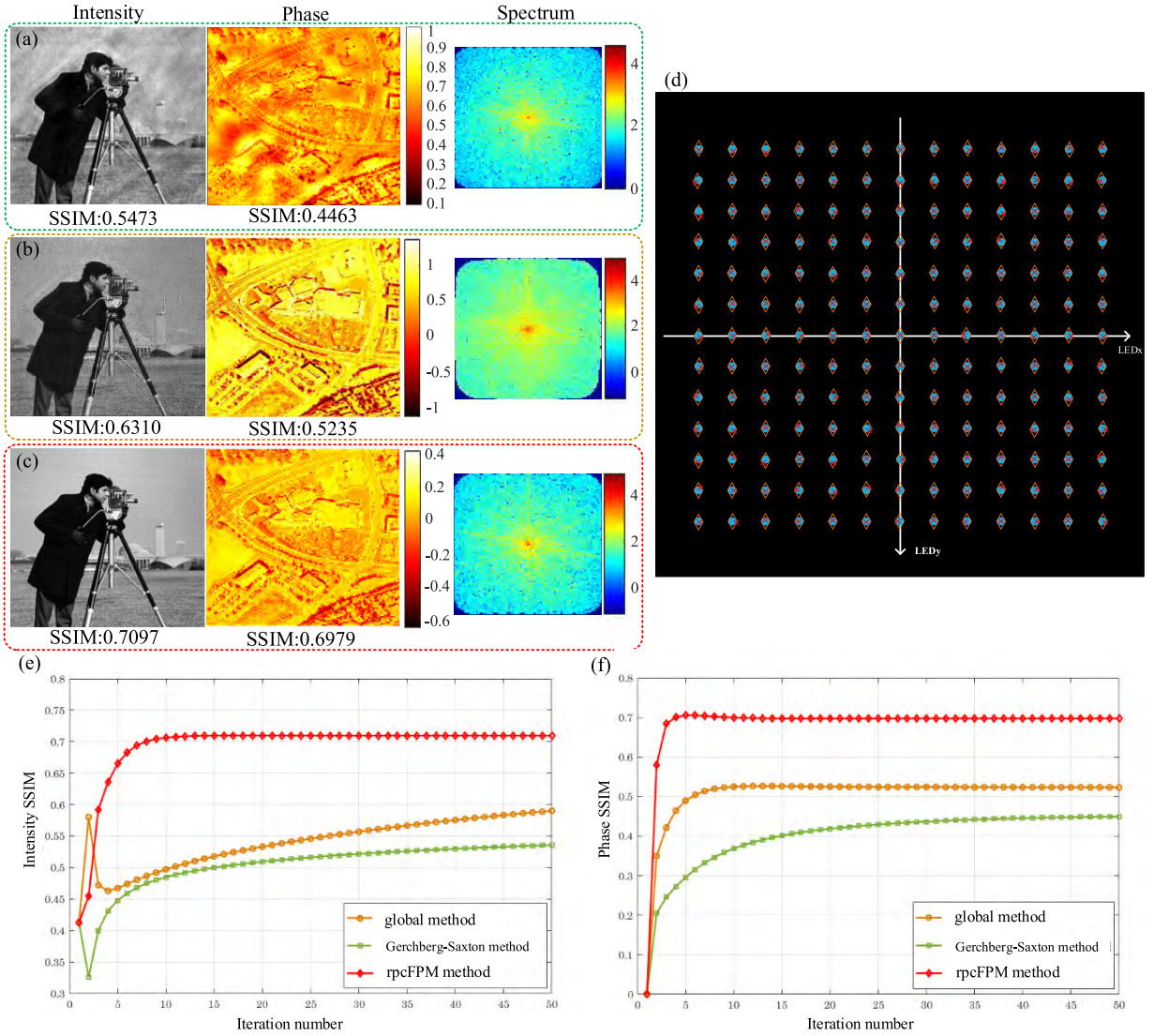

FIGURE 6. The reconstruction results of LR samples with random position deviations using three methods. (a)-(b) The recovered HR intensity, phase images and the central parts of the recovered frequency spectrum respectively with random deviations using Gerchberg-Saxton and global methods. (c) The recovered HR intensity, phase images and the central part of the recovered frequency spectrum respectively with the same deviations condition using rpcFPM method. (d) The position of each LED element in different situations. (e)-(f) The intensity and phase SSIM curves varying with random deviations using three methods.

In this scheme, the initial parameter is set one. And it should be emphasized that it is performed between two adjacent iterations of the object under the same LED element with different positions, which corrects random deviations of each element rather than aligns the misalignment of the whole LED matrix. After K iterations, the random deviations of each LED element are corrected and the corresponding positional shifts $\boldsymbol{\Delta}$ are zero approximately. Besides, a HR complex image can be reconstructed with faster convergence. Moreover, the computational cost can be further reduced due to the decrease of the feedback parameter. In rpcFPM, the convergence and the low-frequency components can be improved correctly because of the recovered DPC phase. And the unknown random positional deviations of each LED element correction attributes to the correlation coefficient value and the feedback parameter.

III. RESULTS

A. SIMULATIONS

We first validate the effectiveness of rpcFPM scheme using simulations before actual experimental data. The simulation parameters are chosen to model a practical FPM platform with an illumination wavelength of 629nm, an image sensor (2160×2560) with pixel size of 6.5μm and a 4× objective with NA of 0.13. We simulate the use of the illumination LED matrix source (13×13) to provide angle-varied illuminations and the distance between the LED matrix and the sample is about 98mm. Similar to the experimental system, 169 LR intensity images are simulated under these parameters. The raw LR complex images are created from the true HR intensity and phase images with 128×128 pixels shown in Fig. 5 (b1) and Fig. 5 (b2). In addition, each position of LED element is added to an artificial random value based

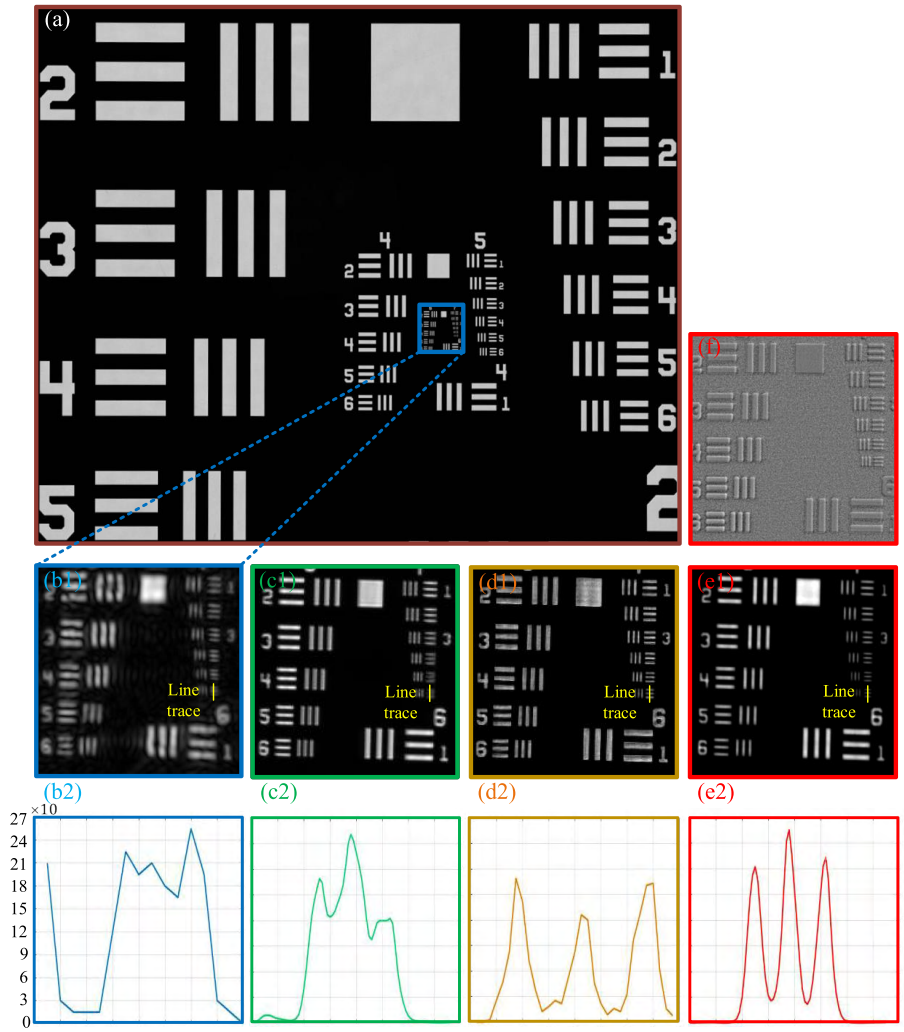

FIGURE 7. Experimental results of the USAF target. (a) The FOV of the USAF target image. (b1) The enlarged ROI. (c1)-(e1) The recovered high-resolution intensities with the Gerchberg-Saxton method, global method, and rpcFPM method respectively. (b2)-(e2) The intensity line traces corresponding to (b1)-(e1). (f) The recovered high-resolution phase with rpcFPM method.

on the standard location (We set the distance between each adjacent LED is 8.128mm without any deviations.). So the simulated LR images are different from these simulated under standard LED matrix. Then, conventional FPM algorithm and rpcFPM algorithm are applied to reconstruct HR intensity and phase images. Here, it is worth mentioning that all of the algorithms use the on-axis-illuminated intensity and DPC recovered phase as the initial guess, which provides a good estimate and faster convergence of the HR complex objective function. Because the artificial random positional deviations of 0-1.5mm are introduced in each LED element, the ideal and erroneous positions are simulated in Fig. 5 (a). As Fig. 5 (a) shows, all of the standard ideal LED positions are marked with red dots while the positions with random positional deviations are marked with green X marks. And we define the first LED is the leftmost and uppermost one as (1, 1). Fig. 5 (c1) and Fig. 5 (c2) show the segment of the central FOV under two positional situations. Fig. 5 (c1) presents the simulated image without random deviations while Fig. 5 (c2) is the image with 0-1.5mm shifting deviations of each LED element. Fig. 5 (d1) and Fig. 5 (d2) show the recovered intensity and phase images without positional deviations correction. It is obvious that the intensity and phase image components in Fig. 5 (d2) are distorted.

Because of the same operation of initial phase acquisition, we just compare the after-reconstruction process of rpcFPM with the Gerchberg-Saxton and global methods using structure similarity (SSIM) as the evaluation criteria to verify the effectiveness of rpcFPM. Then we employ Gerchberg-Saxton, global and rpcFPM methods to reconstruct the HR complex images using raw LR samples with random deviations of each LED element in Fig. 5 (a). Fig. 6 shows the

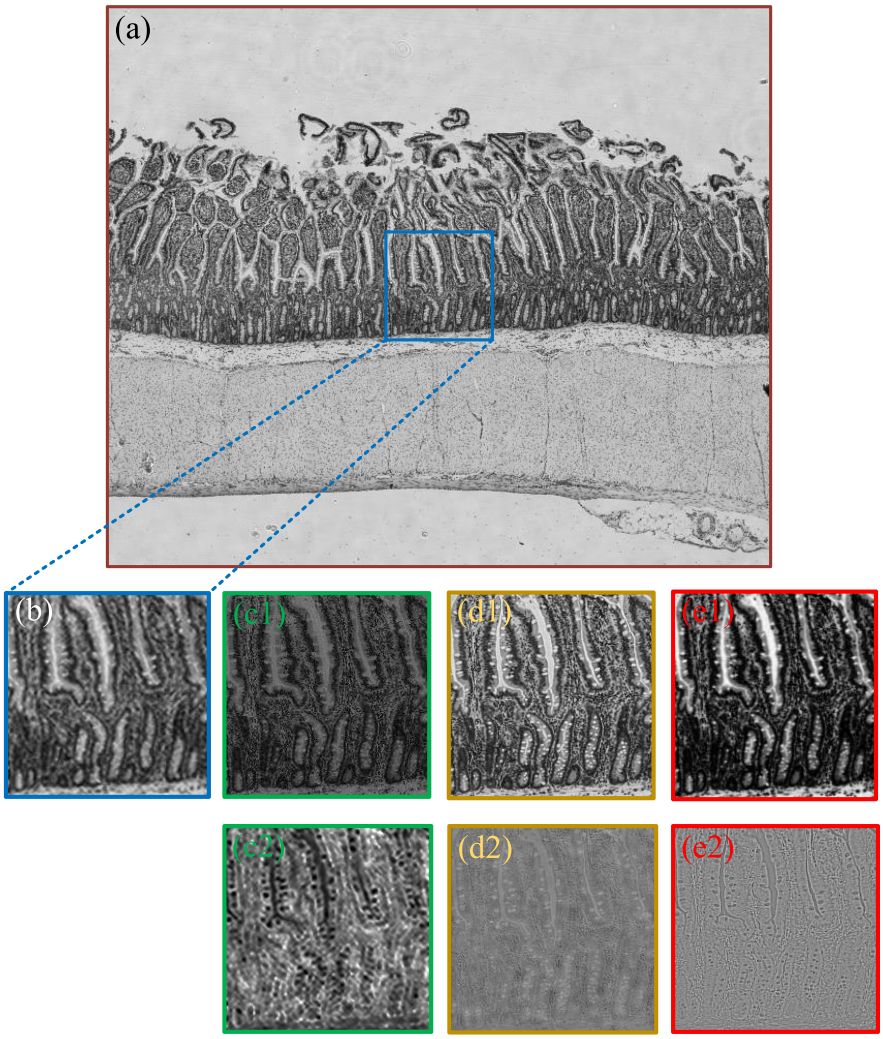

FIGURE 8. Experimental results of a biological intestine tissue. (a) The FOV of the low-resolution intensity specimen. (b) The enlarged ROI in (a). (c1)-(e1) The recovered high-resolution intensities with the Gerchberg-Saxton method, global method, and rpcFPM method respectively. (c2)-(e2) The recovered high-resolution phase images corresponding to (c1)-(e1).

reconstructed results using three methods under the same positional deviations respectively. In Fig. 6 (a)-(c), the iteration stops when the variation of SSIM is less than 0.0001. But in order to compare the rate of convergence, the iteration number is 50 times in Fig. 6 (e)-(f). Fig. 6 (a) and Fig. 6 (b) are the recovered intensity and phase images and the corresponding central parts of the recovered frequency spectrum without LED random deviations correction, while the recovered results with correction using rpcFPM method are shown in Fig. 6 (c). Fig. 6 (d) presents the positions of different LED elements in spatial domain. The uncorrected positions of each LED element with deviations are labeled with red X marks, the actual positions are blue dots and the corrected positions are orange diamonds respectively. For example, after Eq. (10) and Eq. (12), we can get the deviation of (7, 6) LED is $(+0.23mm, +7.348mm)$, the actual position is $(0, -8.128mm)$ and the corrected position is $(+0.063mm, -7.89mm)$. Comparing Fig. 6 (a)-(c), we can see that the random positional deviations of each LED element lead significant errors to the reconstructed HR results. It also can be seen that the reconstructed quality decreases significantly using conventional methods. The SSIM scores between the reconstructed results and the ground truth using rpcFPM are better than the other two methods. Besides, the random deviations of each LED element are corrected and the corrected positions are almost identical to the actual positions in Fig. 6 (d).

Furthermore, the curves of SSIM are used to evaluate the quality of reconstructed results. Fig. 6 (e) and Fig. 6 (f) illustrate the intensity and phase SSIM curves using Gerchberg-Saxton, global and rpcFPM methods to numerically analyze the effectiveness of rpcFPM. It is shown that the SSIM using rpcFPM method is better than others. We also compare the convergence of the three methods used in this

work. It is obvious that rpcFPM nearly reaches the optimal solution after 15 iterations. However, the SSIM of GS and global methods increase gradually and slowly, especially the global method. When the iteration is 50 times, the global method has not been converged. So rpcFPM can increase the convergence and reaches better results. Thus, the simulation results indicate that the FPM reconstructed results are significantly improved after correcting the random positional deviations of each LED element with rpcFPM.

B. EXPERIMENTS

In order to verify the validity of rpcFPM, we experimentally compare the recovered results based on a real FPM platform (Fig. 1). The experimental microscope system is equipped with a 13×13 custom-made LED array (8.128mm between adjacent LED elements) as the angle-varied illuminations to provide 629nm central wavelength. The distance between the sample and the LED array is about 100mm. A set of 169 LR intensity images is imaged with a 4× objective (0.13 NA) and a scientific CMOS (sCMOS) camera with 2560×2160 pixels (6.5μm pixel size). In principle, illumination from each LED is approximately spherical and the final synthetic NA of this system is the sum of objective and the largest angle illumination (approximately 0.7). The exposure time of each sample's image is recorded with 100ms, except the DPC images.

We use an USAF target to quantify the resolution improvement for existing random positional deviations of each LED and positional deviations correction algorithms. Fig. 7 (a) presents the full FOV and LR image and a small region of interest (ROI, 200×200 pixels) is shown in Fig. 7 (b1). Two conventional FPM methods and rpcFPM method are used to reconstruct HR image under the same region and pupil function. Fig. 7 (c1)-(d1) show the recovered HR images without random deviations correction using Gerchberg-Saxton and global methods respectively. Fig. 7 (e1) shows the recovered HR images under the same deviations using rpcFPM method. It can be seen that the recovered HR images in Fig. 7 (c1)-(d1) are distorted because of the random positional deviations. Corresponding to Fig. 7 (b1)-(e1), Fig. 7 (b2)-(e2) are the intensity line traces of the USAF target. We can obviously see that the intensity line trace in Fig. 7 (e2) has the highest contrast with the help of rpcFPM. Comparing with raw image, the resolution all can be improved for each algorithm. However, a better recovered complex image with lower background noise and higher resolution can be achieved by rpcFPM. These results indicate that the random position deviations of each LED can be corrected efficiently and the reconstruction quality can be improved distinctly.

Finally, we also compare rpcFPM with Gerchberg-Saxton and global methods on a biological intestine tissue. Similar to the USAF, Fig. 8 (a) presents the full FOV of the specimen and Fig. 8 (b) shows the corresponding magnified area of interest (200×200 pixels), which is poorly visible and loses valuable details. Fig. 8 (c1)-(d1) and Fig. 8 (c2)-(d2) are the recovered intensity and phase images of Fig. 8 (b) without random positional deviations correction using Gerchberg-Saxton and global methods respectively. Fig. 8 (e1) and Fig. 8 (e2) are the recovered intensity and phase images under the same deviations using rpcFPM method. Though all the algorithms can improve the resolution, Fig. 8 (e1) and Fig. 8 (e2) using rpcFPM achieve higher reconstruction quality, lower noise-included artifacts and outperform the other methods.

IV. CONCLUSION

In this work, we have proposed a random positional deviations correction with initial DPC phase named rpcFPM for FPM reconstruction. It is efficient on time and can decrease the destabilization of the random positional deviations of each LED element. Different from the previous position correction methods for conventional FPM, rpcFPM corrects the random positional deviations of each LED element with a feedback parameter and objective function constraint based on ePIE algorithm and obtains a better initial guess to improve the convergence. Furthermore, comparing with the ordinary FPM, the initial phase of rpcFPM is obtained from DPC method, which can accelerate the convergence and achieve HR phase image with more low-frequency details. Besides, rpcFPM can correct the random positional deviations of each LED element rather than the whole matrix misalignment within iterative process according to the correlation coefficient value. Moreover, rpcFPM can be easily extended by introducing objective function constraint. We also have demonstrated the high-quality of recovered intensity and phase images through simulations and experiments using Gerchberg-Saxton, global and rpcFPM methods. The simulations and experiments all show that rpcFPM can correct the positional deviations adaptively, significantly improve the reconstruction quality of HR complex images and convergent faster than conventional GS and global methods.

Although rpcFPM improves the recovery quality and corrects the random positional deviations of each LED from the results above, it cannot reconstruct the pupil function. Besides, the sampling speed in rpcFPM is still cost-effective. The combination of rpcFPM method and multiplexed coded illumination algorithm may overcome this weakness. Moreover, because this performance is limited by ePIE algorithm, rpcFPM may just reach a local optimum or become a huge calculation-consuming task if each LED has considerably deviations. This appears to be a limitation of our app roach and it will be the subject of future work.

V. ACKNOWLEDGMENT

The authors sincerely acknowledge the editor and the anonymous reviewers for their insightful comments on the manuscript.

REFERENCES

[1] H. M. L. Faulkner and J. M. Rodenburg, "Movable aperture lensless transmission microscopy: A novel phase retrieval algorithm," *Phys. Rev. Lett.*, vol. 93, no. 2, p. 023903, Jul. 2004.

[2] X. Ou, R. Horstmeyer, G. Zheng, and C. Yang, "High numerical aperture Fourier ptychography: Principle, implementation and characterization," *Opt. Express*, vol. 23, no. 3, pp. 3472–3491, 2015.
[3] K. Guo, S. Dong, and G. Zheng, "Fourier ptychography for brightfield, phase, darkfield, reflective, multi-slice, and fluorescence imaging," *IEEE J. Sel. Topics Quantum Electron.*, vol. 2, no. 4, Jul./Aug. 2016, Art. no. 6802712.
[4] J. M. Rodenburg and H. M. L. Faulkner, "A phase retrieval algorithm for shifting illumination," *Appl. Phys. Lett.*, vol. 85, no. 20, pp. 4795–4797, 2004.
[5] A. R. Cohen, F. L. A. F. Gomes, B. Roysam, and M. Cayouette, "Computational prediction of neural progenitor cell fates," *Nature Methods*, vol. 7, pp. 213–218, Feb. 2010.
[6] R. Horstmeyer, R. Y. Chen, X. Ou, B. Ames, J. A. Tropp, and C. Yang, "Solving ptychography with a convex relaxation," *New J. Phys.*, vol. 17, p. 053044, May 2015.
[7] T. R. Hillman, T. Gutzler, S. A. Alexandrov, and D. D. Sampson, "High-resolution, wide-field object reconstruction with synthetic aperture Fourier holographic optical microscopy," *Opt. Express*, vol. 17, no. 10, pp. 7873–7892, 2009.
[8] A. E. Tippie, A. Kumar, and J. R. Fienup, "High-resolution synthetic-aperture digital holography with digital phase and pupil correction," *Opt. Express*, vol. 19, no. 13, pp. 12027–12038, 2011.
[9] P. Gao, G. Pedrini, and W. Osten, "Structured illumination for resolution enhancement and autofocusing in digital holographic microscopy," *Opt. Lett.*, vol. 38, no. 8, pp. 1328–1330, 2013.
[10] R. Gerchberg and W. Saxton, "A practical algorithm for the determination of the phase from image and diffraction plane pictures," *Optik*, vol. 35, no. 2, pp. 237–250, 1972.
[11] R. A. Gonsalves, "Phase retrieval and diversity in adaptive optics," *Opt. Eng.*, vol. 21, no. 5, pp. 829–832, Oct. 1982.
[12] J. R. Fienup, "Phase-retrieval algorithms for a complicated optical system," *Appl. Opt.*, vol. 32, no. 10, pp. 1737–1746, 1993.
[13] M. Guizar-Sicairos and J. R. Fienup, "Phase retrieval with transverse translation diversity: A nonlinear optimization approach," *Opt. Express*, vol. 16, no. 10, pp. 7264–7278, 1993.
[14] A. M. Maiden and J. M. Rodenburg, "An improved ptychographical phase retrieval algorithm for diffractive imaging," *Ultramicroscopy*, vol. 109, no. 10, pp. 1256–1262, 2009.
[15] G. Zheng, R. Horstmeyer, and C. Yang, "Wide-field, high-resolution Fourier ptychographic microscopy," *Nature Photon.*, vol. 7, pp. 739–745, Jul. 2013.
[16] G. Zheng, "Breakthroughs in photonics 2013: Fourier ptychographic imaging," *IEEE Photon. J.*, vol. 6, no. 2, pp. 1–7, Apr. 2014.
[17] S. Pacheco, B. Salahieh, T. Milster, J. J. Rodriguez, and R. Liang, "Transfer function analysis in epi-illumination Fourier ptychography," *Opt. Lett.*, vol. 40, no. 22, pp. 5343–5346, 2015.
[18] J. Chung, X. Ou, R. P. Kulkarni, and C. Yang, "Counting white blood cells from a blood smear using Fourier ptychographic microscopy," *PLoS ONE*, vol. 10, no. 7, p. e0133489, 2015.
[19] A. Williams *et al.*, "Fourier ptychographic microscopy for filtration-based circulating tumor cell enumeration and analysis," *J. Biomed. Opt.*, vol. 19, no. 6, p. 066007, 2014.
[20] L. Tian and L. Waller, "3D intensity and phase imaging from light field measurements in an LED array microscope," *Optica*, vol. 2, no. 2, pp. 104–111, 2015.
[21] L. Tian, X. Li, K. Ramchandran, and L. Waller, "Multiplexed coded illumination for Fourier ptychography with an LED array microscope," *Biomed. Opt. Express*, vol. 5, no. 7, pp. 2376–2389, 2014.
[22] S. Dong, Z. Bian, R. Shiradkar, and G. Zheng, "Sparsely sampled Fourier ptychography," *Opt. Express*, vol. 22, no. 5, pp. 5455–5464, 2014.
[23] L. Bian, J. Suo, G. Situ, G. Zheng, F. Chen, and Q. Dai, "Content adaptive illumination for Fourier ptychography," *Opt. Lett.*, vol. 39, no. 22, pp. 6648–6651, 2014.
[24] L. Bian, J. Suo, G. Zheng, K. Guo, F. Chen, and Q. Dai, "Fourier ptychographic reconstruction using Wirtinger flow optimization," *Opt. Express*, vol. 23, no. 4, pp. 4856–4866, 2015.
[25] J. Zhang, T. Xu, X. Wang, S. Chen, and G. Ni, "Fast gradational reconstruction for Fourier ptychographic microscopy," *Chin. Opt. Lett.*, vol. 15, no. 1, p. 111702, 2017.
[26] X. Ou, G. Zheng, and C. Yang, "Embedded pupil function recovery for Fourier ptychographic microscopy," *Opt. Express*, vol. 22, no. 5, pp. 4960–4972, 2014.
[27] L.-H. Yeh *et al.*, "Experimental robustness of Fourier ptychography phase retrieval algorithms," *Opt. Express*, vol. 23, no. 26, pp. 33214–33240, 2015.
[28] A. M. Maiden, M. J. Humphry, M. C. Sarahan, B. Kraus, and J. M. Rodenburg, "An annealing algorithm to correct positioning errors in ptychography," *Ultramicroscopy*, vol. 120, pp. 64–72, Sep. 2012.
[29] J. Sun, Q. Chen, Y. Zhang, and C. Zuo, "Efficient positional misalignment correction method for Fourier ptychographic microscopy," *Biomed. Opt. Express*, vol. 7, no. 4, pp. 1336–1350, Apr. 2016.
[30] X. Ou, R. Horstmeyer, C. Yang, and G. Zheng, "Quantitative phase imaging via Fourier ptychographic microscopy," *Opt. Lett.*, vol. 38, no. 22, pp. 4845–4848, 2013.
[31] L. Tian, Z. Liu, L.-H. Yeh, M. Chen, J. Zhong, and L. Waller, "Computational illumination for high-speed *in vitro* Fourier ptychographic microscopy," *Optica*, vol. 2, no. 10, pp. 904–911, 2015.
[32] J. Zhang, T. Xu, J. Liu, S. Chen, and X. Wang, "Precise brightfield localization alignment for Fourier ptychographic microscopy," *IEEE Photon. J.*, vol. 10, no. 1, Feb. 2018, Art. no. 6900113.

SINING CHEN is currently pursuing the M.E. degree with the School of Optoelectronics, Beijing Institute of Technology, Beijing, China. Her research interests include computer imaging and Fourier ptychographic microscopy.

TINGFA XU received the Ph.D. degree from the Changchun Institute of Optics, Fine Mechanics and Physics, Changchun, China, in 2004. He is currently a Professor with the School of Optoelectronics, Beijing Institute of Technology, Beijing, China. His research interests include optoelectronic imaging and detection and hyper-spectral remote sensing image processing.

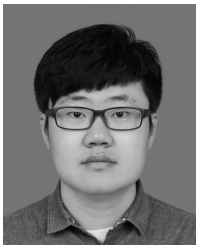

JIZHOU ZHANG received the bachelor's degree from the School of Optics and Photonics, Beijing Institute of Technology, Beijing, China, in 2014, where he is currently pursuing the Ph.D. degree. His research interests include Fourier ptychographic microscopy, computational imaging, and machine learning.

XING WANG is currently pursuing the M.E. degree with the School of Optoelectronics, Beijing Institute of Technology, Beijing, China. Her research interests include computer vision and Fourier ptychographic microscopy.

YIZHOU ZHANG received the master's degree in optical engineering from the Beijing Institute of Technology in 2015, where she is currently pursuing the Ph.D. degree with the Key Laboratory of Optoelectronics Imaging Technology and System of the Education Ministry of China, School of Optics and Photonics. Her research interests include Fourier ptychographic microscopy and infrared image processing.